Cell

Resource

High-Sensitivity Measurements of Multiple Kinase Activities in Live Single Cells

Sergi Regot,[1,*] Jacob J. Hughey,[1] Bryce T. Bajar,[1] Silvia Carrasco,[1] and Markus W. Covert[1,*]
[1]Department of Bioengineering, Stanford University, Stanford, CA 94305, USA
*Correspondence: sregot@stanford.edu (S.R.), mcovert@stanford.edu (M.W.C.)
http://dx.doi.org/10.1016/j.cell.2014.04.039

SUMMARY

Increasing evidence has shown that population dynamics are qualitatively different from single-cell behaviors. Reporters to probe dynamic, single-cell behaviors are desirable yet relatively scarce. Here, we describe an easy-to-implement and generalizable technology to generate reporters of kinase activity for individual cells. Our technology converts phosphorylation into a nucleocytoplasmic shuttling event that can be measured by epifluorescence microscopy. Our reporters reproduce kinase activity for multiple types of kinases and allow for calculation of active kinase concentrations via a mathematical model. Using this technology, we made several experimental observations that had previously been technically-unfeasible, including stimulus-dependent patterns of c-Jun N-terminal kinase (JNK) and nuclear factor kappa B (NF-κB) activation. We also measured JNK, p38, and ERK activities simultaneously, finding that p38 regulates the peak number, but not the intensity, of ERK fluctuations. Our approach opens the possibility of analyzing a wide range of kinase-mediated processes in individual cells.

INTRODUCTION

Ongoing efforts have shown that multicellular systems are best understood as a combination of heterogeneous single-cell behaviors (Lahav et al., 2004; Shankaran et al., 2009; Tay et al., 2010). Intrinsic noise generates cell-to-cell variation that can be critical for cellular survival, development, and differentiation (Balázsi et al., 2011). In response to changing environments, cells also generate complex signaling dynamics that encode relevant information for gene expression, proliferation, or stress responses. Indeed, bulk population dynamics are often qualitatively different from single-cell behaviors (Albeck et al., 2013; Cai et al., 2008; Mettetal et al., 2008; Purvis et al., 2012; Santos et al., 2007).

Dynamic single-cell reporters are essential to study single-cell biology, yet the number of molecular events that can be dynamically monitored in an individual cell are small. Such reporters have led to the successful measurement of metabolic state (Berg et al., 2009), transcription factor localization (Cai et al., 2008), second messenger concentration (Zhao et al., 2011), and even protein activities (Ting et al., 2001; Zhang et al., 2001) in live single cells. In the latter category, kinase activities are of particular interest. It has been estimated that 30% of cellular proteins are phosphorylated on at least one residue (Cohen, 2000; Ptacek et al., 2005). Kinases are known to regulate multiple and diverse biological functions, including the cell cycle, the innate immune response, development, and cell differentiation (Ubersax and Ferrell, 2007).

To date, Förster resonance energy transfer (FRET) sensors have been the most commonly used method to measure kinase activity dynamically in single cells (Fosbrink et al., 2010; Fritz et al., 2013; Ting et al., 2001; Zhang et al., 2001). Such sensors have provided exciting new insights into how kinases are activated in single cells. However, FRET sensors have encountered challenges to their widespread adoption. They often have a low signal-to-noise ratio and do not accurately reflect the downregulation of the kinase, most likely because the closed conformation of the FRET sensor is highly stable, and its phosphorylated sites cannot be accessed by the phosphatases (Komatsu et al., 2011). Perhaps most significantly, they require two fluorescent proteins and thus limit the number of outputs that can be observed simultaneously in any given cell. As signaling networks are known to be highly integrated, it would be highly desirable to measure a particular kinase activity together with multiple other activities or states in the same living cell.

Here, we describe a strategy to generate genetically encoded biosensors for kinase activity named kinase translocation reporters (KTRs). Our approach is based on the concept of converting phosphorylation into a nucleocytoplasmic shuttling event. Although phosphorylation-regulated nucleocytoplasmic translocation in certain specific and naturally occurring proteins has been reported (Gu et al., 2004; Komeili and O'Shea, 1999; Nardozzi et al., 2010) and, in some cases, used as single-cell reporters (Hahn et al., 2009; Hao et al., 2013; Spencer et al., 2013), this concept has never before been exploited to make a general class of synthetic reporters.

We have extensively explored the sequence space and generated a set of rules that allowed us to generate reporters for multiple types of kinases, including mitogen activated protein (MAP)

and AGC kinases. Our method uses a single fluorescent protein for each kinase and reliably recapitulates kinase activity dynamics—both the up- and downregulation—in live single cells. Using KTR technology, we measured c-Jun N-terminal kinase (JNK) activity dynamics in single cells within the context of the innate immune signaling network, showing that different inputs are encoded with different dynamics. Finally, as a proof of principle of the multiplexing capabilities of KTR technology, we have dynamically measured JNK, p38, and ERK activities simultaneously in single living cells and gained insight on how p38 regulates ERK signaling.

RESULTS AND DISCUSSION

A Synthetic Reporter of Kinase Activity Based on Nuclear Translocation

Our initial goal was to construct a single color reporter for JNK activity translating phosphorylation into a localization change. JNK is a central stress-activated protein kinase (SAPK) that coordinates multiple physiological processes like the stress response, innate immune signaling, or development (Bagowski and Ferrell, 2001). We found that the transcription factor c-Jun had a potential nuclear export signal (NES) nearby one of the two major JNK phosphorylation sites (specifically, the S73 site) (Figure 1A). We hypothesized that the phosphorylation state of this site could impact the nuclear export of c-Jun, leading to the conversion of a phosphorylation event into a nucleocytoplasmic shuttling event.

Accordingly, we fused different c-Jun fragments to the fluorescent protein Clover (Lam et al., 2012) and analyzed whether JNK activity (stimulated by the protein synthesis inhibitor anisomycin) altered the localization of any of these constructs. We found that fragments of c-Jun without its C-terminal nuclear localization signal (NLS) have a weak but reproducible localization change from the nucleus to the cytoplasm (Figure 1B). Further fragment analysis revealed that a minimal peptide of 55 amino acids ($Jun^{(29–84)}$), containing the JNK docking site, two phosphorylation sites (S63 and S73), and the identified NES, is sufficient to alter the localization of the fluorescent protein in the presence of anisomycin (Figures 1B, S1A, and S1B available online). This translocation can be blocked with both a specific JNK inhibitor as well as a nonphosphorylatable mutant construct (S73A). We concluded that the shuttling event depends on JNK phosphorylating S73 (Figures 1B, S1C, and S1D). Quantitative western blot analysis revealed that expressing $Jun^{(29–84)}$-Clover does not alter endogenous c-Jun phosphorylation by JNK and that both are phosphorylated and dephosphorylated with similar dynamics (Figures S2A and S2B). Moreover, c-Jun-dependent gene expression remained unaltered in $Jun^{(29–84)}$-Clover-expressing cells (Figure S2C). These results suggested that phosphorylation near the c-Jun NES can enhance nuclear export and that such phosphorylation is being converted into a localization change without changing the endogenous dynamics or consequences of JNK and c-Jun activities.

In order to improve the dynamic range of the observed localization change, we rationally designed a set of mutant variants to explore the sequence space of $Jun^{(29–84)}$ (Figure 1C) (see Supplemental Information for a complete description and analysis). We reasoned that incorporating a negatively regulated NLS (Hahn et al., 2009; Komeili and O'Shea, 1999; Nardozzi et al., 2010) together with the positively regulated NES in the same engineered construct could greatly increase the dynamic range. We began by exploring NES and NLS variants independently. We found that a suboptimal bipartite NLS (bNLS) can be negatively regulated by phosphorylation at either end of the linker region (see Supplemental Information for complete details). In contrast, negatively charged amino acids within the NES sequence increase its basal export activity, which is sufficient to explain why phosphorylation conditionally increases the export rate of the NES.

By combining a negatively phosphoregulated NLS with a positively phosphoregulated NES into a single construct, we were able to increase the dynamic range of nucleocytoplasmic transport by 3-fold (Figures 1D and S2D–S2F and Movie S1). We designated this new construct the JNK kinase translocation reporter (JNK KTR). Importantly, the localization change observed with JNK KTR was readily visible (Figure 1E) and quantifiable (Figure 1F). This localization change could be specifically inhibited by targeting JNK, but not p38 (Figures 1E, 1G, S3A, and S3B). We also observed that a p38 inhibitor caused hyperactivation of JNK KTR (see below for further details). Furthermore, a nonphosphorylatable mutant (JNK KTR^{AA}) localized strictly to the nucleus, whereas a phosphomimetic mutant (JNK KTR^{EE}) was restricted to the cytoplasm, indicating that the negative charge introduced by the phosphorylation is responsible for the change in import and export activities (Figures 1E and S3A).

JNK KTR Dynamics Reflect JNK Activity

To validate the dynamics of JNK KTR, we analyzed JNK activity in response to the cytokine IL-1β as it induces a weaker and more physiological response than anisomycin. IL-1β is a proinflammatory cytokine involved in the innate immune signaling response that activates multiple signaling pathways, including the JNK, p38, and NF-κB pathways (Weber et al., 2010). We compared JNK KTR dynamics with the most common techniques used to detect JNK activity: western blot (WB) (Figure 2A), immunofluorescence (IF) (Figures 2B and 2C) and a FRET-based JNK reporter (JNKAR) (Figures 2D–2F), all in response to the same dose of IL-1β. Results showed that JNK and c-Jun phosphorylation measured by WB or IF strongly correlates with JNK KTR data at both population and single-cell levels (Figures 2A–2C and S3C–S3G). Importantly, the level of JNK KTR expression did not impact the measured cytoplasmic:nuclear (C/N) ratios of the JNK KTR (Figures S3H and S3I). Moreover, in contrast to the JNK KTR data, the JNKAR FRET reporter (Komatsu et al., 2011) measurements failed to capture the downregulation of the kinase (Figure 2F).

To test the functionality of KTR technology in other cell types, we also expressed JNK KTR in HeLa, HEK293, and RAW 264.7 cells. In all cell types, anisomycin induced an expected change in localization (Figure S3J). Taken together, these results suggest that JNK KTR translocation reliably represents JNK activity dynamics and can be successfully implemented in a diverse panel of cell lines.

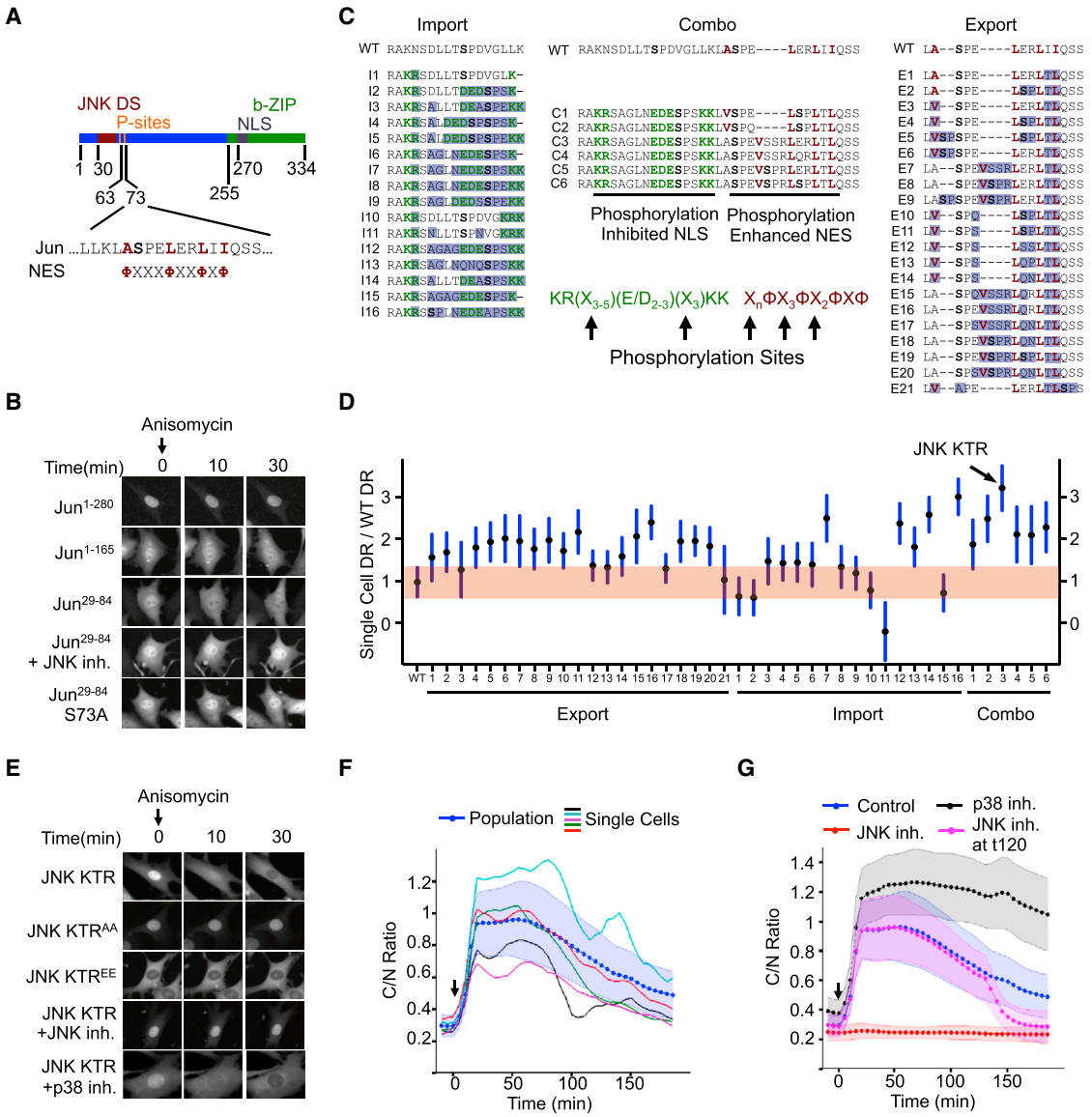

Figure 1. Development of Kinase Translocation Reporter Technology

(A) Schematic representation of mouse c-Jun protein showing JNK docking site (JNK DS), phosphorylation sites (P sites), basic leucine zipper DNA-binding domain (b-ZIP), and NLS. Consensus nuclear export signal (NES, Φ indicates hydrophobic amino acid) and serine 73 sequence context are shown.

(B) 3T3 cells expressing indicated c-Jun fragments fused to Clover were stimulated with anisomycin (50 ng/ml) and imaged at indicated time points. Where indicated (+ JNK inhibitor [inh.]), cells were preincubated for 45 min with 10 μM JNK inhibitor VIII. Representative cells are shown for each construct or condition.

(C) Engineered protein sequences aligned to the wild-type c-Jun sequence. Residues involved in nuclear import, nuclear export, or phosphorylation are shown in green, purple, or bold, respectively. Changes from wild-type sequence are highlighted in blue.

(D) 3T3 cells expressing the Jun$^{29–84}$-Clover variants shown in (C) were treated with anisomycin (50 ng/ml) and imaged over time. Dynamic range was calculated for each cell as (anisomycin-basal)/basal C/N ratio and normalized by the mean wild-type dynamic range. Pink band corresponds to the observed wild-type dynamic range variation. Data are represented as the mean ± SD from more than 50 cells for each variant.

(E) 3T3 cells expressing JNK KTR (WT or with phosphoresidues mutated to alanine, AA, or glutamate, EE) were stimulated with anisomycin (50 ng/ml) and imaged at indicated time points. Where indicated (+ JNK inh. or + p38 inh.), cells were preincubated for 45 min with 10 μM JNK inhibitor VIII or 10 μM SB203580. Representative cells are shown for each construct or condition.

(F) 3T3 JNK KTR cells were stimulated with anisomycin (50 ng/ml), imaged, and quantified as described in the Experimental Procedures. C/N refers to cytoplasmic over nuclear intensities. Data are represented as the mean ± SD from 158 cells.

(G) 3T3 JNK KTR cells were pretreated with 10 μM JNK inhibitor VIII or 10 μM SB203580 (JNK inh. and p38 inh., respectively) and stimulated with anisomycin (50 ng/ml). When indicated (JNK inh. at t120), cells were treated with 10 μM JNK inhibitor VIII. Images were quantified as described in the Experimental Procedures. Data represent mean ± SD from more than 100 cells.

See also Figures S1 and S2.

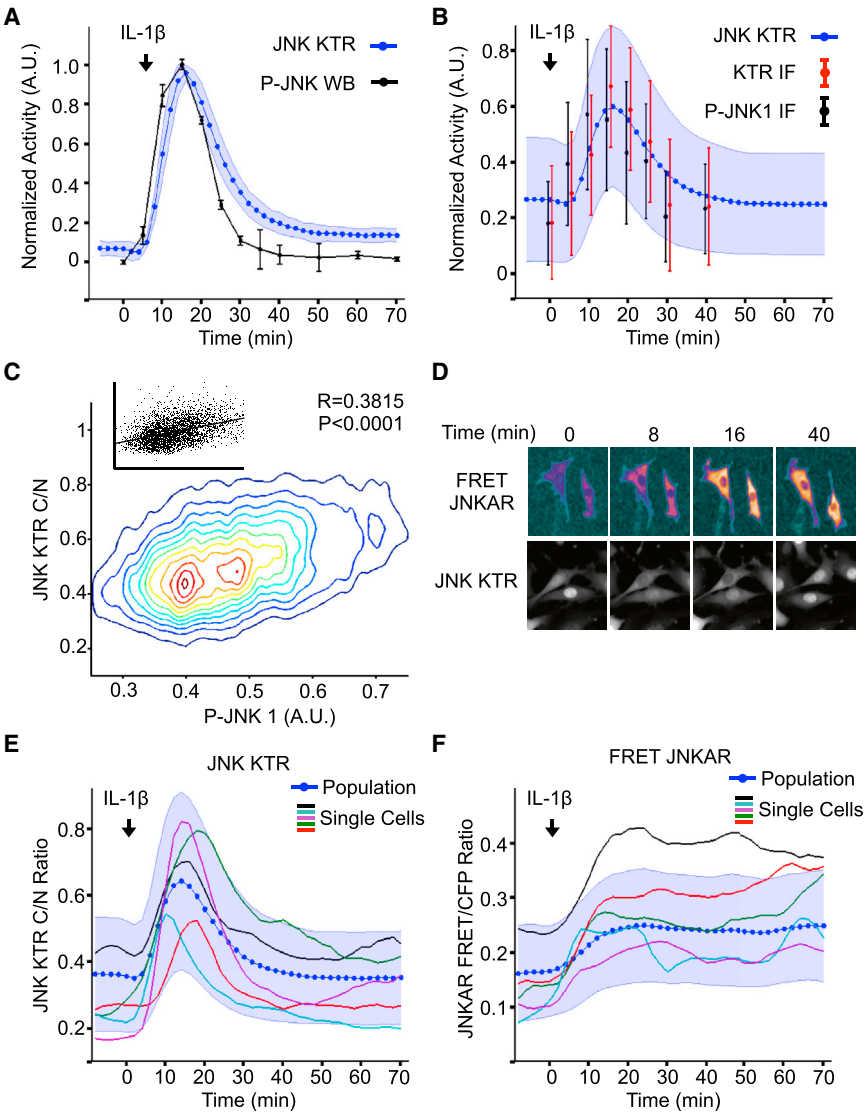

Figure 2. JNK KTR Dynamics Validation

(A) JNK KTR cells were stimulated with IL-1β (1 ng/ml), imaged, and quantified as described in the Experimental Procedures. Three independent experiments were performed, resulting in 980 single cells measured. KTR data represent the mean ± SD from the three experiment means (averaged to mimic in silico WBs). P-JNK WB data are calculated as the fraction of phosphorylated over total and represent the mean ± SD from three independent experiments. All data sets were normalized between 0 and 1 for comparison.

(B) 3T3 JNK KTR cells were stimulated with IL-1β (1 ng/ml) for indicated times and fixed with 4% PFA for quantitative IF analysis. Ten images were taken for each time point and quantified as described in the Experimental Procedures. For each cell, C/N KTR ratio (red) and phospho-JNK intensity (black) were determined. All data sets were normalized between 0 and 1 for comparison. Data represent the mean ± SD from more than 500 cells for each time point obtained from two independent experiments. IF data are overlaid on the dynamic JNK KTR data set (blue) obtained for (A). Note that, in this case, JNK KTR dynamic data represent the mean ± SD from all individual cells (n = 980), obtained in three independent experiments.

(C) IF data obtained in (B) represented as contour scatterplot. Single-cell JNK KTR ratio and phospho-JNK intensity from all time points are shown. Contour color represents areas of increasing data point density. Raw scatterplots fitted to a linear regression are shown together with Pearson correlation value R and P values.

(D) 3T3 JNK KTR cells and 3T3-expressing FRET JNKAR were stimulated with IL-1β (1 ng/ml) and imaged at indicated time points. FRET image was calculated as described in the Experimental Procedures. Representative cells are shown for each technique over time.

(E) 3T3 JNK KTR single-cell dynamic data obtained for (A). Five randomly selected single-cell traces are shown.

(F) FRET JNKAR cells were stimulated with IL-1β (1 ng/ml) imaged and quantified as described in the Experimental Procedures. Data represent the mean ± SD from all individual cells (n = 67) obtained from two independent experiments. Five randomly selected single cell traces are shown.

See also Figure S3.

KTR Technology Can Be Applied to Multiple Types of Kinases

We hypothesized that the design principles we discovered for JNK KTR could be used to generate synthetic single-cell reporters for other kinases. To test this hypothesis, we followed two different strategies, depending on the mechanism of specificity for each kinase. For kinases that operate through distant docking sites (e.g., MAP kinases), we exchanged the JNK docking site with other docking sites found in substrates for other kinases (i.e., Mef2C for p38 and Elk1 for ERK) (Chang et al., 2002). Using this approach, we constructed functional KTRs for ERK and p38 (Figures 3A–3C and S4A–S4C). The KTRs are much more sensitive than the localization of the respective kinase, as we verified with experiments tracking MAP kinase localization (compare Figure 3 with Figures S4D–S4G).

In contrast to MAP kinases, AGC kinases target substrates based on the context of the phosphorylation site. We therefore decided to adapt our KTR construction, mutating a naturally occurring substrate to introduce a bNLS and a NES without interfering with the critical residues for phosphorylation. Using this approach, we converted a fragment of the PKA substrate HDAC8 (which has no localization signals naturally) into a dynamic single-cell reporter (Figure 3D). In each case, the KTR was both responsive and specific to the expected stimulus and inhibitor (Figures 3 and S4C).

These results indicate that KTR technology can be applied to other kinases simply and with minimal optimization. Moreover,

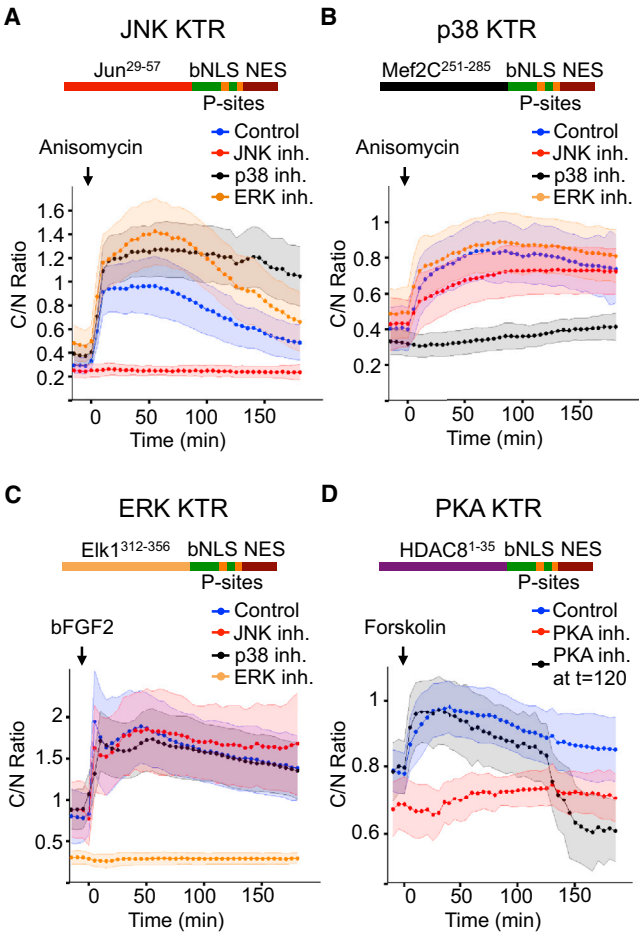

Figure 3. KTR Technology Is Generalizable to Other Kinases

(A) 3T3 cells expressing JNK KTR were stimulated with anisomycin (50 ng/ml), imaged, and quantified as described in the Experimental Procedures. Schematic representation of the engineered reporter is shown for all panels. Data represent the mean ± SD of more than 100 cells. Cells were preincubated with media (control), 10 μM JNK inhibitor VIII (JNK inh.), 10 μM SB203580 (p38 inh.), or 100 nM PD032591 (ERK inh.).

(B) 3T3 cells expressing p38 KTR were stimulated with anisomycin (50 ng/ml), imaged, and quantified as described in the Experimental Procedures. Cells were pretreated or not with kinase inhibitors as in (A).

(C) 3T3 cells expressing ERK KTR were stimulated with basic fibroblast growth factor-2 (bFGF2, 100 ng/ml), imaged, and quantified as described in the Experimental Procedures. Cells were pretreated or not with kinase inhibitors as in (A).

(D) 3T3 cells expressing PKA KTR were stimulated with the PKA activator forskolin (10 μM) imaged and quantified as described in the Experimental Procedures. Cells were pretreated with the specific PKA inhibitor H89 (30 μM) (+ PKA inh.) or not (control). Where indicated, H89 (30 μM) was added at time 120 min (+ PKA inh. at t = 120).

See also Figure S4.

recently reported mammalian CDK2 and yeast PKA kinase reporters (Hao et al., 2013; Spencer et al., 2013) have the same naturally occurring arrangement of bNLS, NES, and phosphorylation sites in their sequences. As a result, the KTR strategy has been successful for three classes of kinases (MAPKs, CDKs, and AGC kinases), suggesting that the technology is generalizable.

Calculating the Single-Cell Concentration of Active Kinase via a Mathematical Model

The KTR technology offered an exciting new possibility to estimate, quantitatively, the concentrations of active kinase in individual cells. To do this, we used the chemical reactions of the KTR (phosphorylation, dephosphorylation, import, and export) to construct a mathematical model of the system (see supplemental equations in the Extended Experimental Procedures for details). The model describes the quantitative relationship between the dynamics of active kinase and the dynamics of the KTR. We then calibrated the model specifically for the JNK KTR (Figure 4A). To estimate the import and export rate constants of the unphosphorylated and phosphorylated states of the KTR, we treated cells expressing the nonphosphorylatable JNK KTR^{AA} or the phosphomimetic JNK KTR^{EE} construct with the nuclear export inhibitor leptomycin B (Figures S5A and S5B).

Importantly, a similar approach to estimate concentrations of active kinase in single cells could not be used with FRET sensors. This is because no method is currently known for producing a constitutively phosphomimetic FRET sensor, and without such a control, it is impossible to know the fraction of active wild-type sensor. As a result, critical parameters of the system remain unspecified. In contrast, the phosphomimetic construct required for KTR models is straightforward to implement and leads to novel calculations of active kinase concentration.

In addition to providing the import and export rate constants, the JNK KTR^{AA} and the JNK KTR^{EE} constructs also give us the expected C/N ratio of the wild-type JNK KTR if 0% or 100% of the wild-type JNK KTR molecules in a cell were phosphorylated. For a KTR to be most useful and for accurate estimation of active kinase concentrations, the KTR should be responsive to the range of active kinase concentrations under baseline and stimulated conditions. Based on our parameterization with the JNK KTR^{AA} and JNK KTR^{EE} constructs, we calculated the relationship between active JNK concentration and steady state C/N ratio (Figure 4B). Interestingly, JNK KTR reaches only about 80% saturation in response to IL-1β, TNF- α, and LPS. We conclude that the responsive range of the JNK KTR is almost ideally matched to the range of active JNK induced by physiological stimuli.

We noticed that all four of the nonphosphorylatable JNK KTR mutants (JNK KTR^{AA}, JNK KTR^{AE}, JNK KTR^{EA}, and JNK KTR^{EE}) exhibited a similar degree of cell-to-cell variability in the C/N ratio (Figure S5C). In addition, the C/N ratios of two different nonphosphorylatable mutants in the same cell were highly correlated (Figures S5D and S5E). This suggests that variability in the C/N ratio of the wild-type JNK KTR and all other KTRs is caused not only by variability in levels of active kinase but also by noise in the import and export rates. To distinguish between these two sources of variability in individual cells, we generated a cell line expressing both JNK KTR-Clover and an in-cell control construct, JNK KTR^{AE}-mRuby2 (Lam et al., 2012) (Figures 4C, S5D, and S5E). Although this construct cannot be phosphorylated, the bNLS and NES signals are still functional. As a result, the C/N ratio variability is caused strictly by differences in general import and export rates.

Surprisingly, although the C/N ratios of two nonphosphorylatable mutants (JNK KTR^{AE} and JNK KTR^{EA}) correlated well in

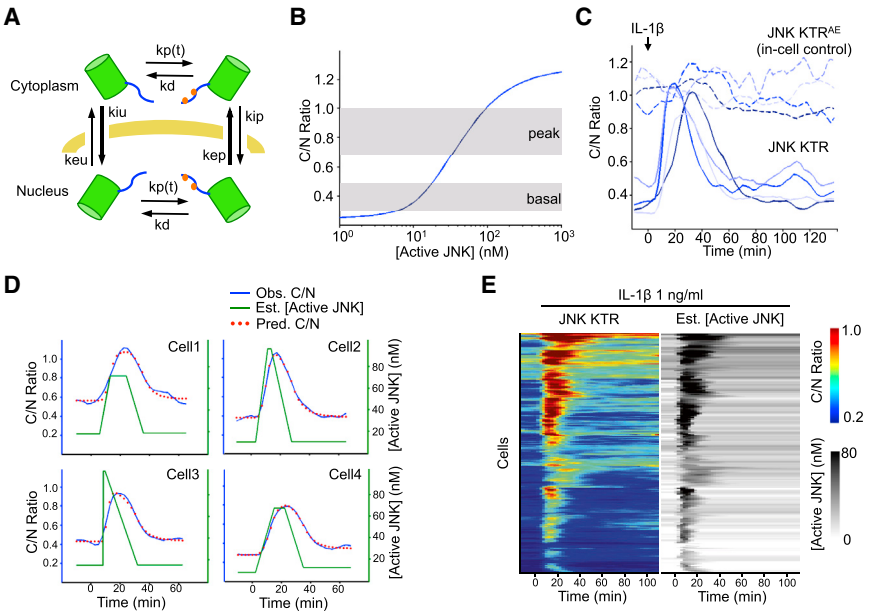

Figure 4. KTR Modeling Allows Estimating Active JNK Kinase Concentration in Single Cells

(A) Schematic representation of the mathematical model, see the supplemental equations in the Extended Experimental Procedures for a complete description of the parameters depicted in this figure.

(B) Model-based relationship between steady-state C/N JNK KTR ratio and concentration of active JNK. Gray areas indicate the range of C/N ratios observed (at basal or peak times) when cells are stimulated with 1 ng/ml IL-1β (data represent the distribution of C/N ratio between 25th and 75th percentiles).

(C) 3T3 cells expressing JNK KTR Clover (solid line) and JNK KTR^{AE}mRuby2 (super index indicates A and E mutations on the phosphorylation sites) (dashed line) were stimulated with IL-1β (1 ng/ml), imaged, and quantified as described in the Experimental Procedures. The activation dynamics for each protein in four randomly chosen individual cells are shown.

(D) Cells were treated as in (C). Observed C/N ratio (blue line), estimated active kinase concentration obtained as described in the Experimental Procedures (green line), and fitted C/N ratio using the estimated concentration of active kinase for that particular cell (red dots) are shown for four randomly chosen individual cells.

(E) Cells were treated as in (B). Each row of the heat map corresponds to an individual cell. Corrected JNK KTR C/N ratio and estimated concentration of active JNK are displayed in tandem for each cell. No normalization was used for the corrected JNK KTR C/N ratio. Heat maps represent 195 cells and two independent experiments.

See also Figure S5.

single cells, the C/N ratios of JNK KTR^{AE} and wild-type JNK KTR correlated very weakly (Figures S5D and S5E). This observation suggests that the variability of the wild-type JNK KTR is primarily caused not by noise in import and export rates but by variability in basal JNK activity. A similar finding has been made in yeast, where basal MAP kinase activity has been shown to accelerate the response time of the high osmolarity glycerol (HOG1) pathway (Macia et al., 2009). However, little is known about this phenomenon in mammalian MAPK pathways.

We also observed the dynamics of the wild-type JNK KTR and in-cell control in response to IL-1β. Our subsequent analysis showed that nuclear import and export noise is negligible compared to the localization change induced by JNK activation (Figure 4C). We then used the model to estimate the concentration of active kinase over time in single cells (Figures 4D, 4E, and S5F–S5H, see supplemental equations in the Extended Experimental Procedures for details). Our analysis suggests that the baseline concentration of active JNK is between 0 and 15 nM, and that, upon treatment with IL-1β, active JNK concentration peaks between 20 and 80 nM (Figure S5G). Consistent with the data from western blots (Figures 2A, S2A, S2B, S3C, and S3D), the C/N ratio of the JNK KTR closely tracks the estimated concentration of active JNK (Figures 4D and 4G).

Taken together, these results indicate that, for most applications, the C/N ratio of the wild-type KTR, even without an in-cell control, is a sensitive and accurate proxy for kinase activity. However, the in-cell control remains useful for generating more accurate calculations of kinase activity in single cells. In addition, the in-cell control can also be used to compare ratios between cell lines and to calibrate the system when a stimulus affects general import or export rates. Finally, the simplicity of the KTR model structure, as well as the straightforward, standardizable method for model parameterization all suggest that the method could be readily applied to other KTRs to obtain active kinase concentrations in single cells.

KTR Technology Applied to Novel Biological Measurements

Finally, we were anxious to use KTR technology to perform novel measurements—in particular, multifactorial analysis of live single cells. We first investigated how JNK and the transcription factor NF-κB act in a coordinated fashion to generate specificity in innate immune signaling. Accordingly, we introduced JNK KTR-mCerulean3 (Markwardt et al., 2011) into previously described *RelA*$^{-/-}$ 3T3 p65-DsRed H2B-EGFP cells (Tay et al., 2010) and isolated a clonal line. We then stimulated cells with three different innate immune inputs (TNF-α, IL-1β, and LPS), spanning three orders of magnitude in concentration, and measured p65 and JNK KTR nucleocytoplasmic translocation dynamics in each individual cell (Figures 5A, 5B, and S6). Translocation of JNK KTR (indicating activation of JNK) was transient in most cells, with a time to peak that correlated well with the time to peak of nuclear p65 (Figures 5B and 5C). In particular, for both JNK KTR and p65, the timing of the response was slower for LPS than for either TNF-α or IL-1β. In addition, in response to TNF-α and IL-1β, JNK KTR translocation tended to precede p65 translocation by 6–12 min—a finding made possible by the fine time resolution offered by KTR technology.

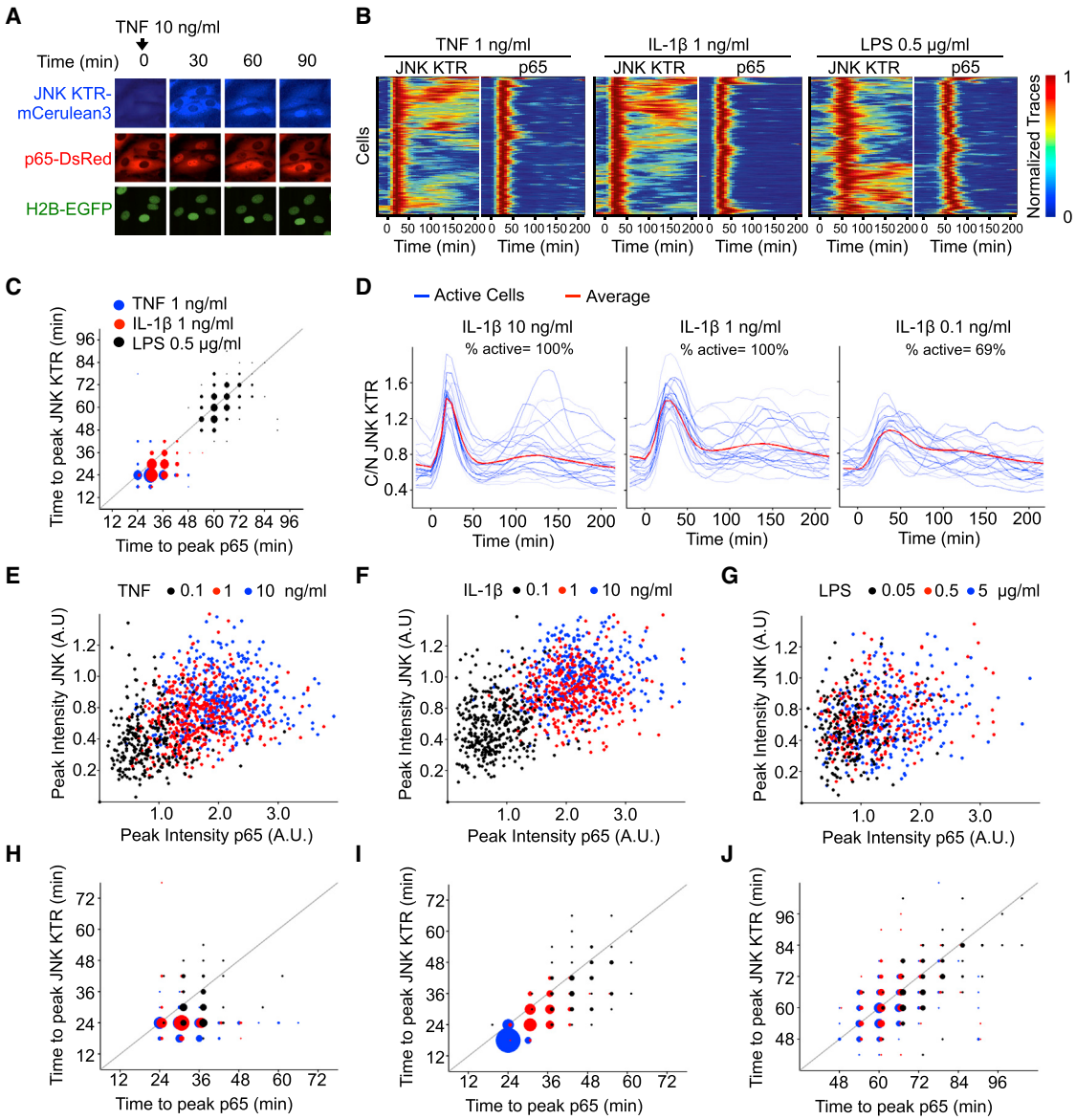

Figure 5. KTR Technology Provides a New Dimension for Analyzing the Innate Immune Signaling Network

(A) *RelA*$^{-/-}$ 3T3 cells expressing H2B-EGFP and p65-DsRed were infected with JNK KTR-mCerulean3, and a clonal cell line was isolated (cell line 3B8). 3B8 cells were stimulated with TNF-α (10 ng/ml) and imaged at indicated times. Representative cells are shown for each channel over time.

(B) Clonal line 3B8 was stimulated with the indicated concentration of TNF-α, IL-1β, or LPS, imaged, and quantified as described in the Experimental Procedures. Each row of the heat map corresponds to a single cell; JNK KTR and nuclear p65 (p65) dynamics are displayed in tandem for each cell (>300 cells total, three independent experiments), with each trace normalized between 0 and 1 for each reporter.

(C) The amount of time elapsed at the first peak of activity for JNK KTR and p65-dsRed. Data come from (B), and dot size represents the number of cells. Gray line indicates x = y.

(D) Clonal line 3B8 was stimulated with indicated concentrations of IL-1β, imaged, and quantified as described in methods. Twenty-five randomly chosen cells (blue) and the average of all cells (>300) (red) are shown.

(E–J) 3B8 cells were stimulated with indicated concentrations of TNF-α (E and H), IL-1β (F and I), or LPS (G and J). Correlations between JNK KTR and p65 peak amplitude (E, F, and G) or time to first peak (H, I, and J) are shown. Dot size represents the number of cells. Gray line indicates x = y.

See also Figures S6 and S7.

At the single-cell level, we found that the JNK response varied between cells, most notably in the basal state (i.e., unstimulated cells growing in 1% calf serum), as well as during downregulation of activity (Figures 5D and S6). We also observed that JNK KTR oscillated in some, but not all, cells upon stimulation with TNF-α or IL-1β (Figures 5D, S7A, and S7B). These findings would have been very difficult or impossible to obtain using population assays, which blend together asynchronous cellular responses,

or using the JNK FRET sensor, which is too slow in reporting downregulation of JNK (Figure 2F).

Detailed 2D analysis of the single-cell response—taking JNK and p65 simultaneously into account—showed that the amplitude and the time to the first peak of JNK and p65 are differently used to encode dose at the single-cell level. For example, stimulation with either TNF-α or IL-1β yields JNK and p65 peak intensities that are positively correlated with one another across ligand concentration (Figures 5E and 5F). In contrast, cells respond to LPS with timing that is independent of concentration and without correlation between peak JNK and p65 amplitudes (Figure 5G).

The correlation between the timing of the response for JNK and p65 was different. In this case, the time to the first peak of activity for both reporters seemed to be correlated and dose dependent under both LPS and IL-1β stimulation conditions, but not for TNF-α (Figures 5H–5J). These data strongly suggest that multiple innate immune inputs can be differently interpreted by the same signaling network by generating different dynamic patterns of key effectors.

Finally, as MAP kinases are known to regulate each other, we explored how the three MAP kinases JNK, ERK, and p38 dynamically interact in single cells. Accordingly, we generated a cell line expressing four different fluorescent proteins (4C cell line): ERK KTR-Clover, p38 KTR-mCerulean3, JNK-KTR-mRuby2, and H2B-tdiRFP (Filonov et al., 2011) (Figure 6A). This cell line allowed us to simultaneously measure the activity dynamics of all three MAP kinases in single cells over entire cell cycles (Figure 6B). Our data confirmed that ERK activity in NIH 3T3 cells fluctuates under basal conditions with dynamics similar to those previously described in MCF-10 cells (Albeck et al., 2013) (Figure 6B). Interestingly, previous studies (Shankaran et al., 2009) showed periodic oscillations of extracellular signal-regulated kinase (ERK) localization upon epidermal growth factor (EGF) stimulation. However, in NIH 3T3 cells, the basal fluctuations are visible only with ERK KTR, as ERK localization itself does not oscillate (Figures S4F and S4G). This observation highlights the utility of using KTR technology as a more direct assessment of kinase activity.

Moreover, our data suggest that the basal activity of both ERK and p38 correlates with the cell cycle. In particular, we found that ERK fluctuations are more frequent in the beginning of the cell cycle, whereas basal activation of p38 tends to be higher toward the end of the cell cycle (Figure 6C).

Next, we considered the interactions between the kinases. Using experiments at the population level, others have previously described the inhibition of ERK by p38 (Jensen et al., 2013; Westermarck et al., 2001). This inhibition is important because p38 has been shown to regulate cell-cycle progression (Joaquin et al., 2012). Therefore, a better understanding of how p38 regulates ERK can provide some insight into how SAP kinases regulate the cell cycle. To study this interaction at the single-cell level, we measured the dynamics of ERK, p38, and JNK activation in response to anisomycin. Upon anisomycin treatment, activation of JNK was more transient than activation of p38 (Figure 6D). Moreover, after treatment with anisomycin, inhibition of JNK only affected JNK, whereas inhibition of p38 caused an increase in both JNK and ERK activities. These results suggest that p38 activity represses both the ERK and JNK pathways (Figure 6E).

Furthermore, the single-cell analysis revealed that p38 inhibits ERK fluctuations by reducing the number of peaks rather than their intensity (Figures 6F, S7C, and S7D). Given that the time between ERK fluctuations has been shown to encode proliferation signals (Albeck et al., 2013), ERK inhibition by p38 provides a plausible mechanism for cell-cycle regulation upon stress. These observations demonstrate that KTR technology has an unprecedented potential to enable the generation of multidimensional data sets.

In summary, KTR technology is an easy-to-implement, generalizable strategy for developing reporters of kinase activity in live cells. We have shown how KTRs enable measurement of single-cell activation dynamics of multiple signaling pathways simultaneously and with high time resolution. Furthermore, construction and parameterization of a mathematical model to represent KTR activity is both mathematically and experimentally straightforward and enables the estimation of active kinase concentrations. Although we emphasize that FRET sensors remain powerful tools in this area, particularly in their capacity to elucidate the subcellular distribution of kinase activity, the multiplexing capabilities of KTR technology open the possibility of measuring single-cell dynamics of signaling networks rather than signaling pathways by relatively simple and cost-effective means. We anticipate that this strategy will contribute significantly to our understanding of the mechanisms underlying dynamic signal transduction in individual living cells.

EXPERIMENTAL PROCEDURES

Cell Line Generation

Engineered sequences were generated by Gibson assembly (Gibson et al., 2009) into pENTR vectors and then sequenced and transferred to pLenti DEST vectors using Gateway Cloning Technology. Lentiviral vectors were transfected into a 293FT cell line together with third generation packaging plasmids. Packaged lentivirus was used to infect 3T3s 48 hr later. Drug selection was added (Puromycin 1 μg/ml, Blasticidin 1 μg/ml, or Hygromycin 50 μg/ml [InvivoGen]) 24 hr postinfection. Cells were imaged to confirm fluorescent protein expression 3–5 days later.

Cells were cultured in Dulbecco's modified Eagle's medium (DMEM) (Invitrogen) supplemented with 2 mM L-glutamine (GIBCO), 100 U/ml penicillin, 100 μg/ml streptomycin (GIBCO), and 10% fetal bovine serum (Omega Scientific) or calf serum (Colorado). Derivates of *RelA*$^{-/-}$ 3T3 were cultured in 10% FBS, whereas derivates of NIH 3T3 were cultured in 10% FCS.

Imaging

Cells were seeded at 7,000 cells/well onto glass coverslip 96-well plates (Nunc) coated with 10 μg/ml fibronectin (Millipore). The next day, media were changed to imaging media (DMEM without phenol red with 1% FBS or FCS, see above) at least 1 hr prior to imaging. Cell lines without a genetically encoded nuclear marker were incubated with 50 ng/ml Hoechst (Sigma) to assist nuclear segmentation. Cells were imaged with a Nikon Eclipse Ti fluorescence microscope controlled by Micromanager (Edelstein et al., 2010). Temperature (37°C), CO_2 (5%), and humidity were held constant during the experiments. Five blank positions (media only) were imaged for every experiment and used to flat field the rest of the images.

Image Quantification

Flatfielding and image registration were performed using custom Matlab software. Segmentation and object quantification was performed with CellProfiler (Kamentsky et al., 2011). Nucleus and a five-pixel-wide cytoplasm ring

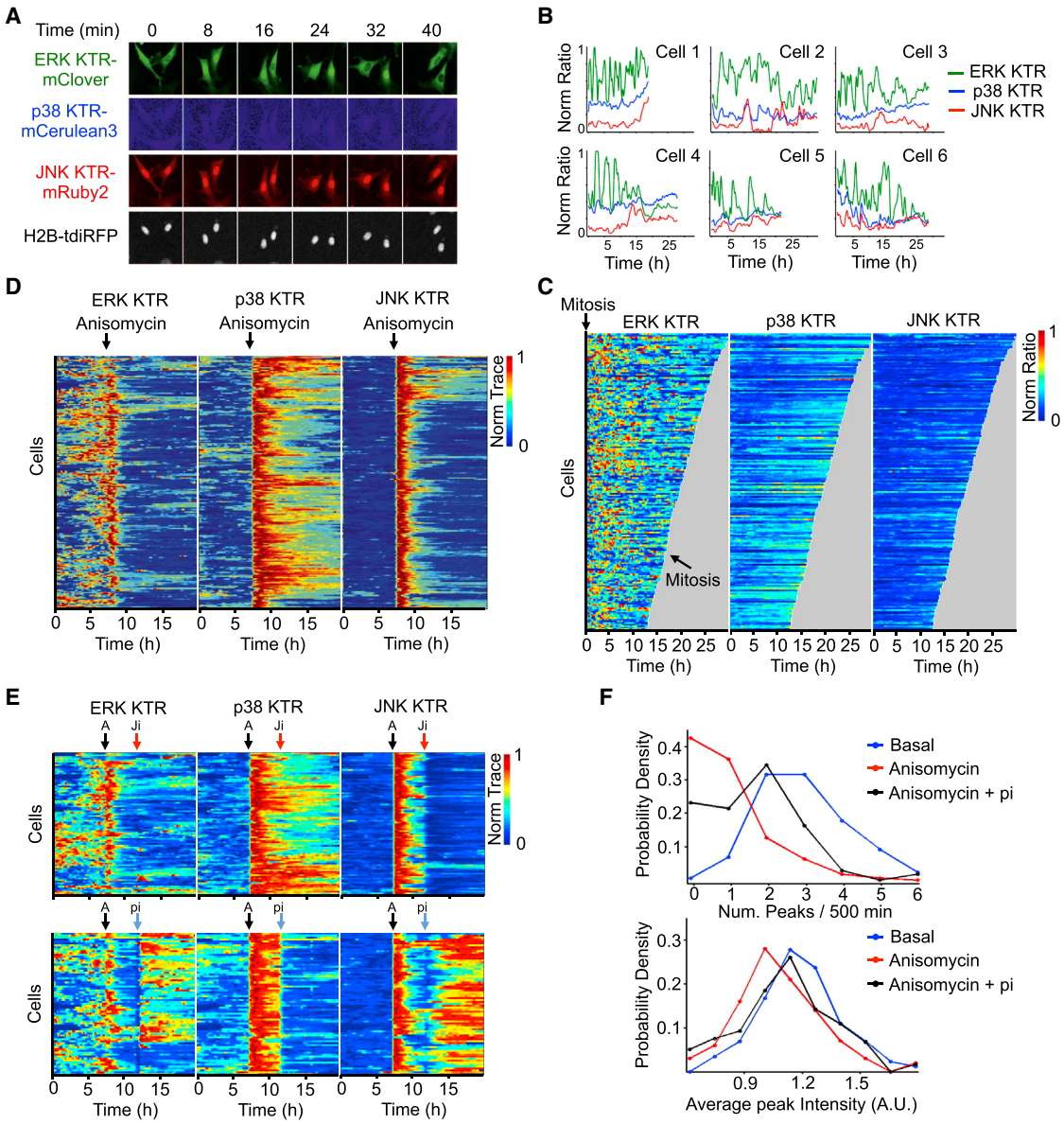

Figure 6. KTR Technology Allows Output Multiplexing

(A) 3T3 cells expressing indicated fusion proteins (4C cell line) were imaged under basal conditions over time. Representative cells are shown for each time point.

(B and C) 4C cell line was imaged every 8 min without stimulation and quantified as described in the Experimental Procedures without stimulation. Six representative cells (B) and heat maps for 196 cells (C) are shown. For each cell, ERK, p38, and JNK KTRs were quantified from mitotic exit to mitotic entry.

(D and E) 4C cell line was stimulated with Anisomycin (A) (50 ng/ml) where indicated (black arrow) and treated with 10 μM JNK inhibitor VIII (Ji) or 10 μM SB203580 (pi) (red or blue arrows, respectively). Images were taken every 8 min and quantified as described in Methods. Heat maps for more than 100 cells are shown.

(F) Peaks of ERK activity from data presented in (C) and (E) were identified using custom software. Distributions of number of peaks per 500 min (top) and average peak intensity (bottom) are shown for three conditions; no stimuli (blue), Anisomycin 50 ng/ml (red), or Anisomycin 50 ng/ml and 10 μM SB203580 (pi) (black).

See also Figure S7.

(cytoring) were segmented for each cell using Hoechst or H2B fused fluorescent proteins and quantified in each channel. Tracking and manual curation were performed using custom Matlab and Python software. Median intensity values for each object were extracted and used to calculate ratios. KTRs cytoring over nuclear intensities were calculated to intuitively reflect activity. Nuclear p65 intensity was normalized using the cytoplasmic intensity under basal conditions. For Figures 1D and S2D–S2F, basal and 30 min postanisomycin cytoplasmic over nuclear ratio was quantified. Dynamic range was calculated for each cell as (anisomycin-basal)/basal C/N ratio and normalized by the mean wild-type dynamic range. For heat maps shown in Figures 5B, 6C, and 6E, each trace was normalized between 0 and 1. When more than one KTR was compared (Figures 6D and 6E), each trace was normalized using as

minimum and maximum the inhibitor and stimulated mean ratios obtained in Figure 3.

FRET Analysis

For FRET JNKAR experiments, H2B-mRuby2 3T3 cells were transfected with JNKAR1EV plasmid (Komatsu et al., 2011) (kindly donated by Dr. Kazuhiro Aoki) 24 hr prior to imaging. The mRuby2 image was used to segment the nuclei. YFP, CFP, and FRET images were taken and corrected for signal bleed through as previously described (Feige et al., 2005). FRET image was divided by CFP image, and the resulting image was used to quantify FRET signal in the cytoplasm.

Immunofluorescence

Cells were seeded at 12,000 cells/well onto glass coverslip 8-well imaging slides (Lab-tek) coated with 10 μg/ml fibronectin (Millipore). The next day, media were changed to imaging media (DMEM without phenol red with 1% FBS or FCS) at least 1 hr prior to stimulation. Cells were stimulated for indicated times, fixed with 4% paraformaldehyde, and permeabilized with PBS 0.5% Triton X-100. Blocking and antibody incubations were done in PBG buffer (PBS, 0.2% cold water fish gelatin [Sigma], 0.5% BSA [Sigma]). Phospho-SAPK/JNK (Thr183/Tyr185) (81E11) Rabbit mAb (4668, Cell Signaling) and Phospho-c-Jun (Ser63) II Antibody (9261, Cell Signaling) were used as primary antibodies. Goat anti-Rabbit (Cy5) (ab97077, abcam) secondary antibody was used to detect primary antibodies. 10 ng/ml DAPI was used to stain the nuclei for segmentation purposes. Ten multichannel images (DAPI, mClover, and Cy5) were taken for each IF condition. Images were segmented as described above, and median intensities for mClover and Cy5 channels were obtained. JNK phosphorylation was calculated as the sum of nuclear and cytoplasmic intensities, whereas JUN phosphorylation corresponded to nuclear Cy5 intensity.

Quantitative Western Blotting

Cells were grown to 80% confluence onto six-well plates, and media were changed to 1% FBS or FCS media for 1 hr prior to stimulation. After stimulation, cells were harvested, and proteins were extracted in 150 μl of RIPA buffer containing protease and phosphatase inhibitors. Proteins were resolved in 4%–12% gradient SDS PAGE gels (BioRad) and transferred into low autofluorescence PVDF membranes (Millipore). Blocking and antibody incubations were done with LICOR blocking buffer. The primary antibodies used were as follows: Phospho-SAPK/JNK (Thr183/Tyr185) (81E11) Rabbit (4668, Cell Signaling), Phospho-c-Jun (Ser63) Rabbit (9261, Cell Signaling), Phospho-c-Jun (Ser73) Antibody (9164, Cell Signaling), JNK1 (2C6) Mouse (3708, Cell Signaling), c-Jun (5B1) Mouse (ab119944, abcam), and GFP Rabbit (ab290, abcam). Membranes were scanned using a LICOR scanner and quantified using ImageStudioLite software.

Quantitative Gene Expression Analysis

Cells were grown to 80% confluence onto six-well plates, and media were changed to 1% FBS or FCS media for 1 hr prior to stimulation. After stimulation, cells were harvested, and RNA was extracted using RNeasy Mini Kit (74104 Quiagen). cDNA was produced using High Capacity cDNA Reverse Transcription Kit with RNase Inhibitor (4374966, Applied Biosystems). Quantitative PCR was performed using Taqman gene expression assay (Life Technologies).

SUPPLEMENTAL INFORMATION

Supplemental Information includes Extended Experimental Procedures, seven figures, and one movie and can be found with this article online at http://dx.doi.org/10.1016/j.cell.2014.04.039.

AUTHOR CONTRIBUTIONS

S.R. conceived the initial idea for KTR technology. S.R, B.T.B., S.C., and M.W.C. did the experiments. J.J.H. implemented the model and performed the mathematical analysis presented in Figure 4. S.R., J.J.H., and M.W.C. wrote the paper. M.W.C. supervised the project.

ACKNOWLEDGMENTS

We thank S. Collins and members of the Covert lab, in particular D. Macklin, for helpful discussions and comments on the manuscript. We thank Dr. K. Aoki for providing the FRET-based JNKAR plasmid. We also gratefully acknowledge a Human Frontier Science Program (HFSP) postdoctoral fellowship (LT000529/2012-L) to S.R., as well as an NIH R21 (5R21AI104305-02), an NIH Pioneer Award (5DP1LM01150-05), the Stanford Center for Systems Biology (NIH P50GM107615), and an Allen Distinguished Investigator Award to M.W.C. S.R., J.J.H., and M.W.C. are listed as inventors in a patent application for KTR technology.

Received: January 2, 2014
Revised: March 19, 2014
Accepted: April 25, 2014
Published: June 19, 2014

REFERENCES

Albeck, J.G., Mills, G.B., and Brugge, J.S. (2013). Frequency-modulated pulses of ERK activity transmit quantitative proliferation signals. Mol. Cell *49*, 249–261.

Bagowski, C.P., and Ferrell, J.E., Jr. (2001). Bistability in the JNK cascade. Curr. Bio. *11*, 1176–1182.

Balázsi, G., van Oudenaarden, A., and Collins, J.J. (2011). Cellular decision making and biological noise: from microbes to mammals. Cell *144*, 910–925.

Berg, J., Hung, Y.P., and Yellen, G. (2009). A genetically encoded fluorescent reporter of ATP:ADP ratio. Nat. Methods *6*, 161–166.

Cai, L., Dalal, C.K., and Elowitz, M.B. (2008). Frequency-modulated nuclear localization bursts coordinate gene regulation. Nature *455*, 485–490.

Chang, C.I., Xu, B.E., Akella, R., Cobb, M.H., and Goldsmith, E.J. (2002). Crystal structures of MAP kinase p38 complexed to the docking sites on its nuclear substrate MEF2A and activator MKK3b. Mol. Cell *9*, 1241–1249.

Cohen, P. (2000). The regulation of protein function by multisite phosphorylation—a 25 year update. Trends Biochem. Sci. *25*, 596–601.

Filonov, G.S., Piatkevich, K.D., Ting, L.M., Zhang, J., Kim, K., and Verkhusha, V.V. (2011). Bright and stable near-infrared fluorescent protein for in vivo imaging. Nat. Biotechnol. *29*, 757–761.

Fosbrink, M., Aye-Han, N.N., Cheong, R., Levchenko, A., and Zhang, J. (2010). Visualization of JNK activity dynamics with a genetically encoded fluorescent biosensor. Proc. Natl. Acad. Sci. USA *107*, 5459–5464.

Fritz, R.D., Letzelter, M., Reimann, A., Martin, K., Fusco, L., Ritsma, L., Ponsioen, B., Fluri, E., Schulte-Merker, S., van Rheenen, J., and Pertz, O. (2013). A versatile toolkit to produce sensitive FRET biosensors to visualize signaling in time and space. Sci. Signal. *6*, rs12.

Gibson, D.G., Young, L., Chuang, R.Y., Venter, J.C., Hutchison, C.A., 3rd, and Smith, H.O. (2009). Enzymatic assembly of DNA molecules up to several hundred kilobases. Nat. Methods *6*, 343–345.

Gu, J., Xia, X., Yan, P., Liu, H., Podust, V.N., Reynolds, A.B., and Fanning, E. (2004). Cell cycle-dependent regulation of a human DNA helicase that localizes in DNA damage foci. Mol. Biol. Cell *15*, 3320–3332.

Hahn, A.T., Jones, J.T., and Meyer, T. (2009). Quantitative analysis of cell cycle phase durations and PC12 differentiation using fluorescent biosensors. Cell Cycle *8*, 1044–1052.

Hao, N., Budnik, B.A., Gunawardena, J., and O'Shea, E.K. (2013). Tunable signal processing through modular control of transcription factor translocation. Science *339*, 460–464.

Jensen, K.J., Garmaroudi, F.S., Zhang, J., Lin, J., Boroomand, S., Zhang, M., Luo, Z., Yang, D., Luo, H., McManus, B.M., and Janes, K.A. (2013). An ERK-p38 subnetwork coordinates host cell apoptosis and necrosis during coxsackievirus B3 infection. Cell Host Microbe *13*, 67–76.

Joaquin, M., Gubern, A., González-Nuñez, D., Josué Ruiz, E., Ferreiro, I., de Nadal, E., Nebreda, A.R., and Posas, F. (2012). The p57 CDKi integrates stress

signals into cell-cycle progression to promote cell survival upon stress. EMBO J. *31*, 2952–2964.

Komatsu, N., Aoki, K., Yamada, M., Yukinaga, H., Fujita, Y., Kamioka, Y., and Matsuda, M. (2011). Development of an optimized backbone of FRET biosensors for kinases and GTPases. Mol. Biol. Cell *22*, 4647–4656.

Komeili, A., and O'Shea, E.K. (1999). Roles of phosphorylation sites in regulating activity of the transcription factor Pho4. Science *284*, 977–980.

Lahav, G., Rosenfeld, N., Sigal, A., Geva-Zatorsky, N., Levine, A.J., Elowitz, M.B., and Alon, U. (2004). Dynamics of the p53-Mdm2 feedback loop in individual cells. Nat. Genet. *36*, 147–150.

Lam, A.J., St-Pierre, F., Gong, Y., Marshall, J.D., Cranfill, P.J., Baird, M.A., McKeown, M.R., Wiedenmann, J., Davidson, M.W., Schnitzer, M.J., et al. (2012). Improving FRET dynamic range with bright green and red fluorescent proteins. Nat. Methods *9*, 1005–1012.

Macia, J., Regot, S., Peeters, T., Conde, N., Solé, R., and Posas, F. (2009). Dynamic signaling in the Hog1 MAPK pathway relies on high basal signal transduction. Sci. Signal. *2*, ra13.

Markwardt, M.L., Kremers, G.J., Kraft, C.A., Ray, K., Cranfill, P.J., Wilson, K.A., Day, R.N., Wachter, R.M., Davidson, M.W., and Rizzo, M.A. (2011). An improved cerulean fluorescent protein with enhanced brightness and reduced reversible photoswitching. PLoS ONE *6*, e17896.

Mettetal, J.T., Muzzey, D., Gómez-Uribe, C., and van Oudenaarden, A. (2008). The frequency dependence of osmo-adaptation in Saccharomyces cerevisiae. Science *319*, 482–484.

Nardozzi, J.D., Lott, K., and Cingolani, G. (2010). Phosphorylation meets nuclear import: a review. Cell Commun. Signal. *8*, 32.

Ptacek, J., Devgan, G., Michaud, G., Zhu, H., Zhu, X., Fasolo, J., Guo, H., Jona, G., Breitkreutz, A., Sopko, R., et al. (2005). Global analysis of protein phosphorylation in yeast. Nature *438*, 679–684.

Purvis, J.E., Karhohs, K.W., Mock, C., Batchelor, E., Loewer, A., and Lahav, G. (2012). p53 dynamics control cell fate. Science *336*, 1440–1444.

Santos, S.D., Verveer, P.J., and Bastiaens, P.I. (2007). Growth factor-induced MAPK network topology shapes Erk response determining PC-12 cell fate. Nat. Cell Biol. *9*, 324–330.

Shankaran, H., Ippolito, D.L., Chrisler, W.B., Resat, H., Bollinger, N., Opresko, L.K., and Wiley, H.S. (2009). Rapid and sustained nuclear-cytoplasmic ERK oscillations induced by epidermal growth factor. Mol. Syst. Biol. *5*, 332.

Spencer, S.L., Cappell, S.D., Tsai, F.C., Overton, K.W., Wang, C.L., and Meyer, T. (2013). The proliferation-quiescence decision is controlled by a bifurcation in CDK2 activity at mitotic exit. Cell *155*, 369–383.

Tay, S., Hughey, J.J., Lee, T.K., Lipniacki, T., Quake, S.R., and Covert, M.W. (2010). Single-cell NF-kappaB dynamics reveal digital activation and analogue information processing. Nature *466*, 267–271.

Ting, A.Y., Kain, K.H., Klemke, R.L., and Tsien, R.Y. (2001). Genetically encoded fluorescent reporters of protein tyrosine kinase activities in living cells. Proc. Natl. Acad. Sci. USA *98*, 15003–15008.

Ubersax, J.A., and Ferrell, J.E., Jr. (2007). Mechanisms of specificity in protein phosphorylation. Nat. Rev. Mol. Cell Biol. *8*, 530–541.

Weber, A., Wasiliew, P., and Kracht, M. (2010). Interleukin-1 (IL-1) pathway. Sci. Signal. *3*, cm1.

Westermarck, J., Li, S.P., Kallunki, T., Han, J., and Kähäri, V.M. (2001). p38 mitogen-activated protein kinase-dependent activation of protein phosphatases 1 and 2A inhibits MEK1 and MEK2 activity and collagenase 1 (MMP-1) gene expression. Mol. Cell. Biol. *21*, 2373–2383.

Zhang, J., Ma, Y., Taylor, S.S., and Tsien, R.Y. (2001). Genetically encoded reporters of protein kinase A activity reveal impact of substrate tethering. Proc. Natl. Acad. Sci. USA *98*, 14997–15002.

Zhao, Y., Araki, S., Wu, J., Teramoto, T., Chang, Y.F., Nakano, M., Abdelfattah, A.S., Fujiwara, M., Ishihara, T., Nagai, T., and Campbell, R.E. (2011). An expanded palette of genetically encoded Ca^{2+} indicators. Science *333*, 1888–1891.